Stem Cell Reports, Volume *17*

Supplemental Information

Aggregation of cryopreserved mid-hindgut endoderm for more reliable and reproducible hPSC-derived small intestinal organoid generation

Amy L. Pitstick, Holly M. Poling, Nambirajan Sundaram, Phillip L. Lewis, Daniel O. Kechele, J. Guillermo Sanchez, Melissa A. Scott, Taylor R. Broda, Michael A. Helmrath, James M. Wells, and Christopher N. Mayhew

Figure S1, related to Figure 1

A.

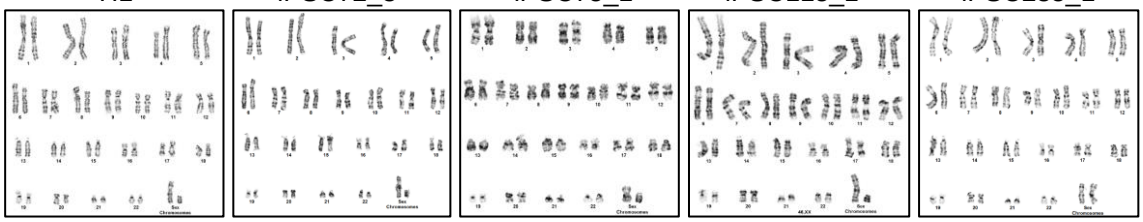

B.

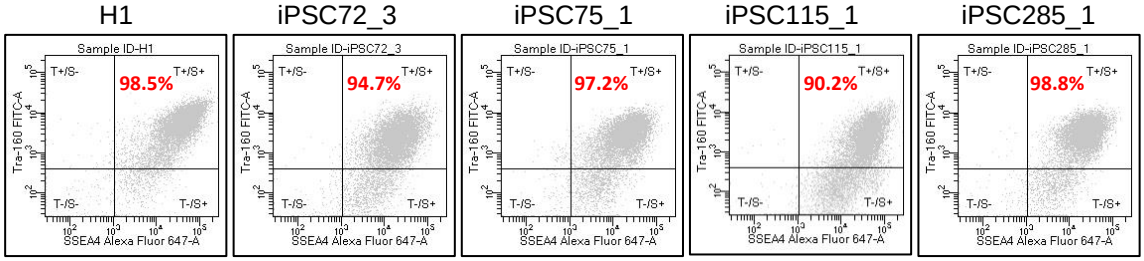

C.

	D3S1358	TH01	D21S11	D18S51	Penta E	D5S818	D13S317	D7S820	D16S539	CSF1PO	Penta D	vWA	D8S1179	TPOX	FGA	AMEL
H1	15	9.3	28, 32.2	17, 18	10, 12	9, 11	8, 11	8, 12	9, 13	12, 13	10, 13	15, 17	12, 13	8, 11	20, 24	X, Y
iPSC72_3	16, 18	9.3	30, 30.2	15, 18	13	12	9, 12	10, 11	11, 13	10	12, 13	15, 17	11, 14	8, 11	24	X, Y
iPSC75_1	18	9	28, 30	17, 21	13, 14	10, 12	8, 14	8, 14	10, 11	11, 12	9	16, 17	13, 16	9, 11	21, 25	X, Y
iPSC115_1	15	9.3	31.2, 32.2	17, 18	5, 16	9, 13	11, 12	8, 12	13	12	9, 12	14, 17	11, 13	8, 11	21, 24	X, Y
iPSC295_1	17, 18	6, 9.3	30, 31.2	11, 16	12	11, 12	11, 14	11, 12	9, 11	12, 13	9, 12	14	11, 12	8, 11	20, 24	X

D.

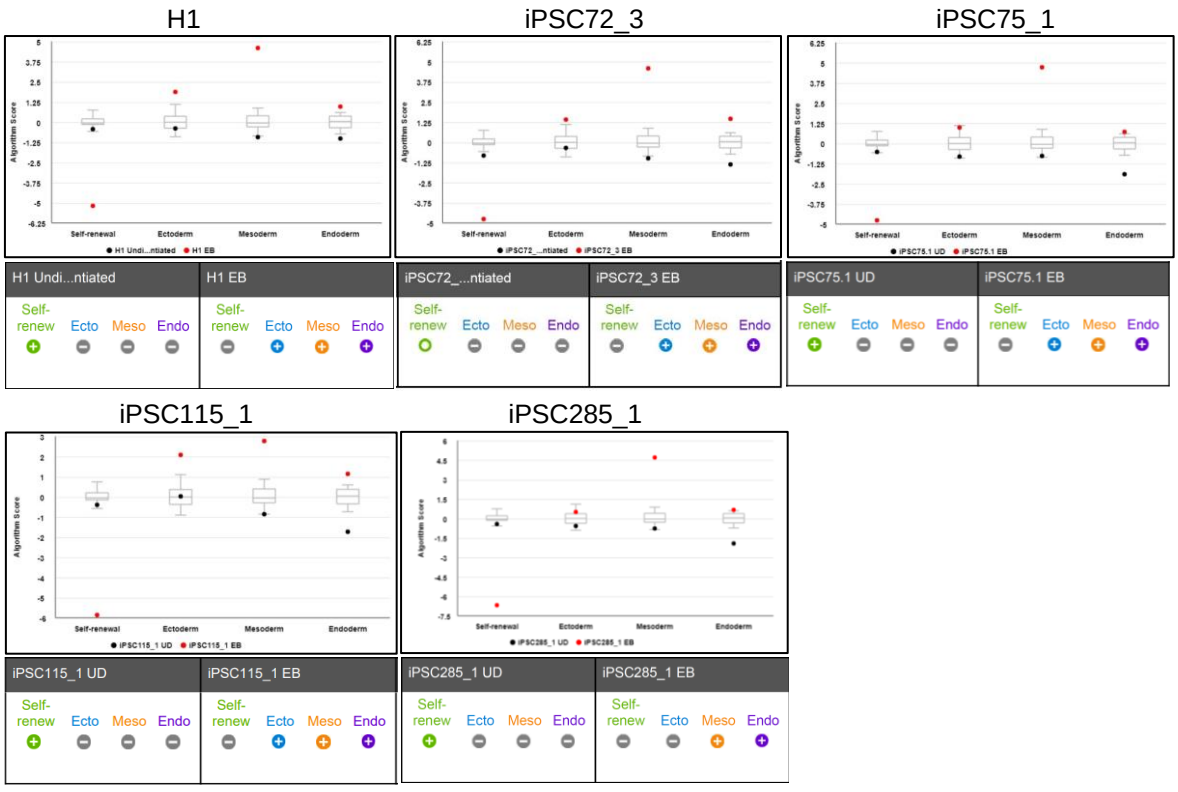

Figure S2, related to Figures 1 and 5

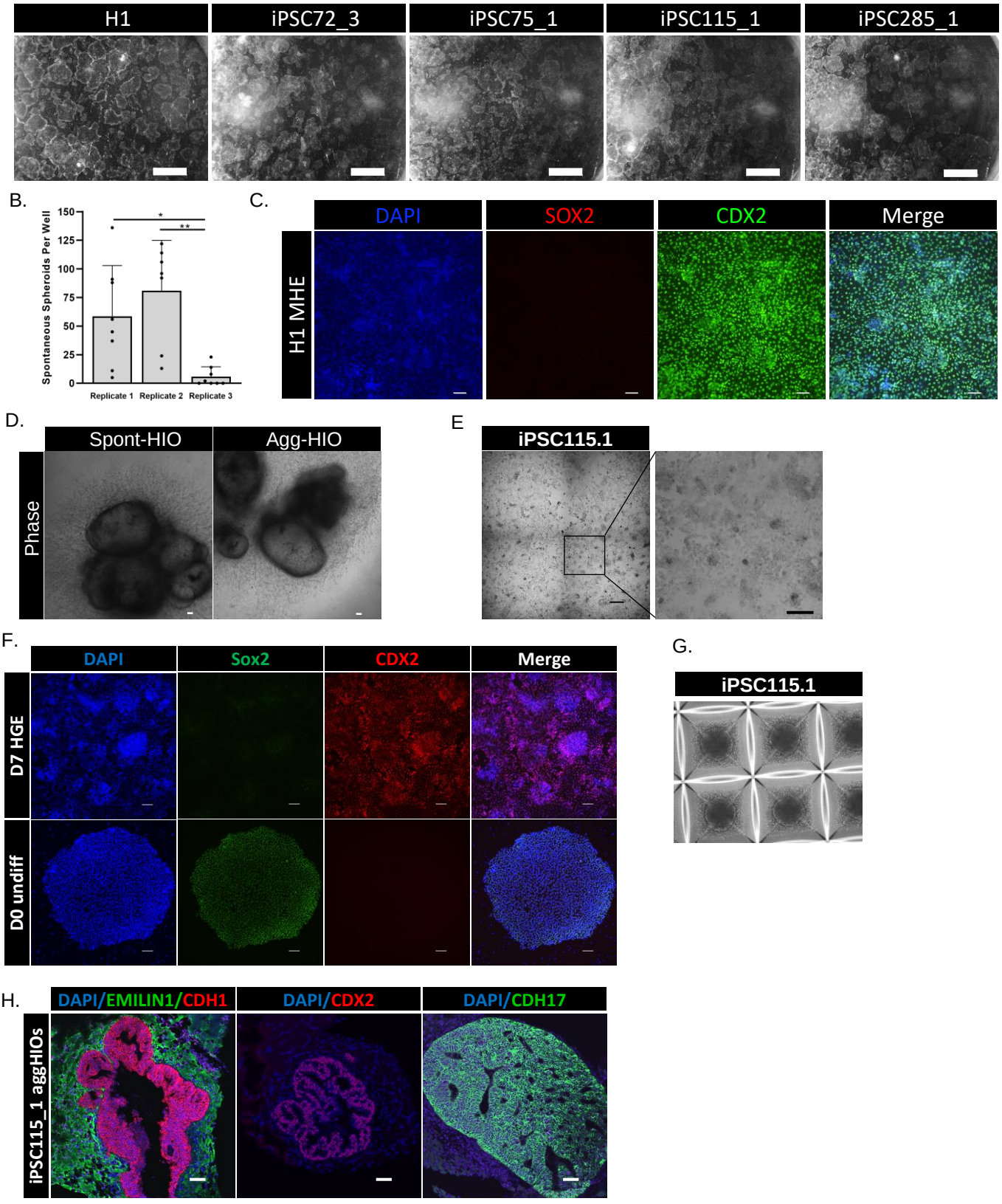

Figure S3. related to Figure 3

A.

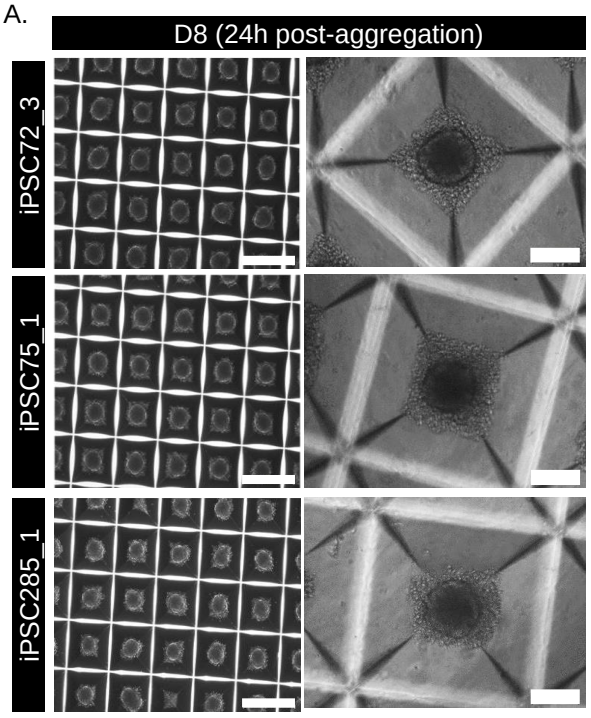

B.

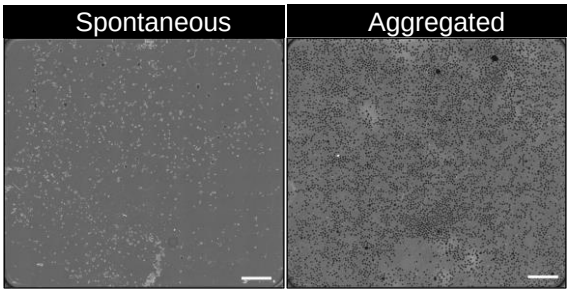

C.

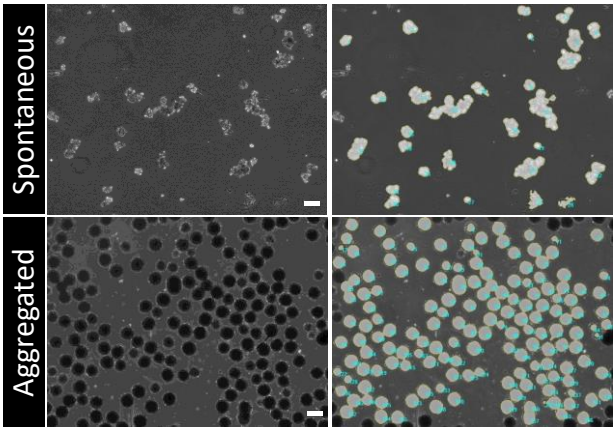

D.

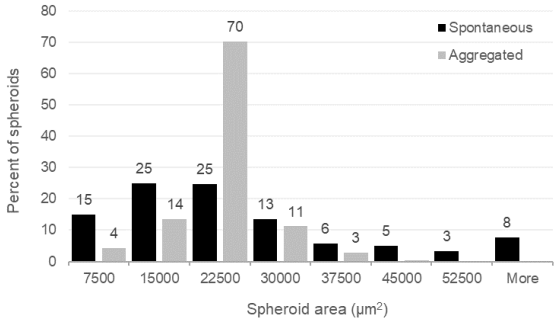

Figure S4, related to Figures 4 and 5

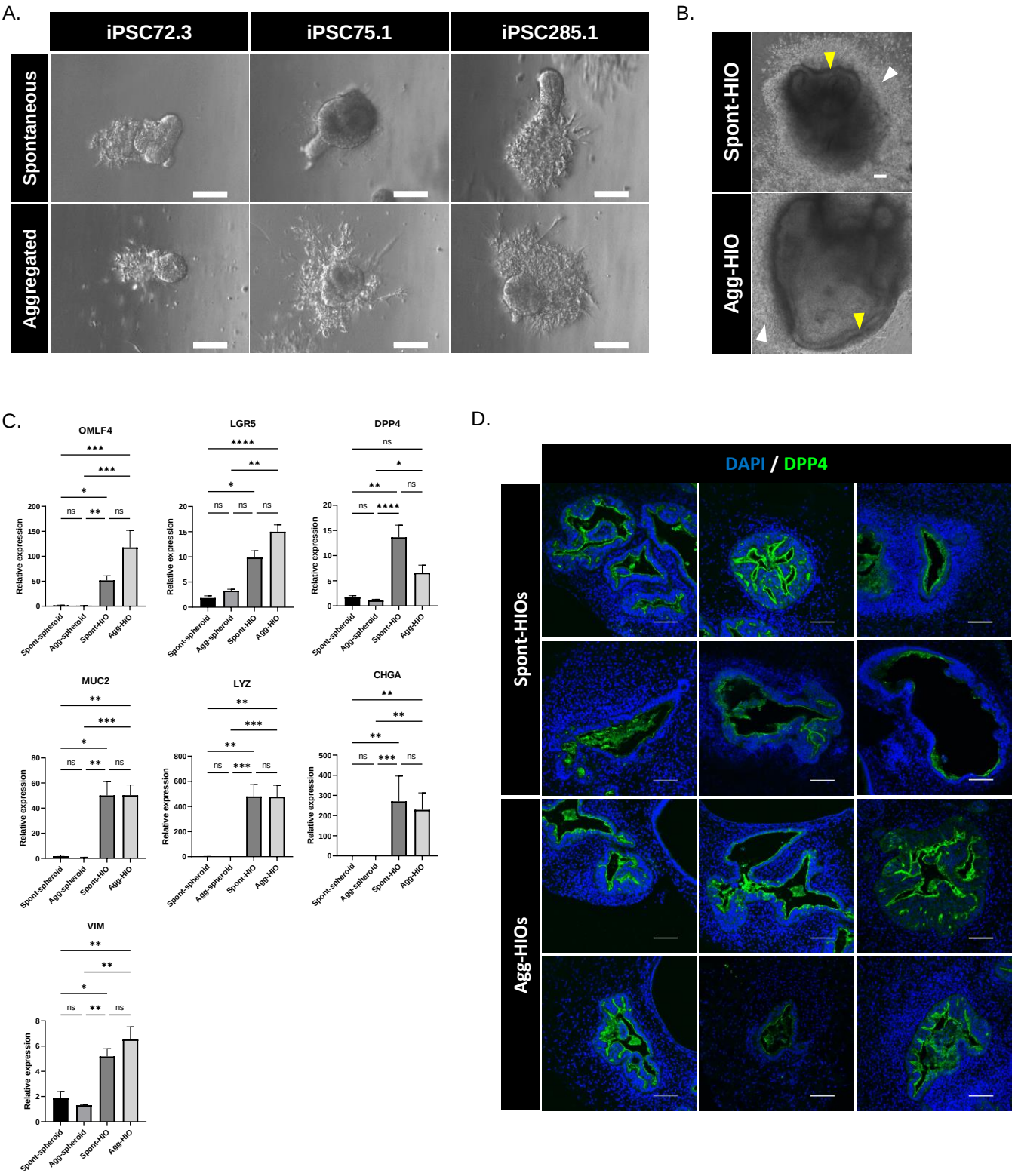

Figure S5, related to Figure 5

A.

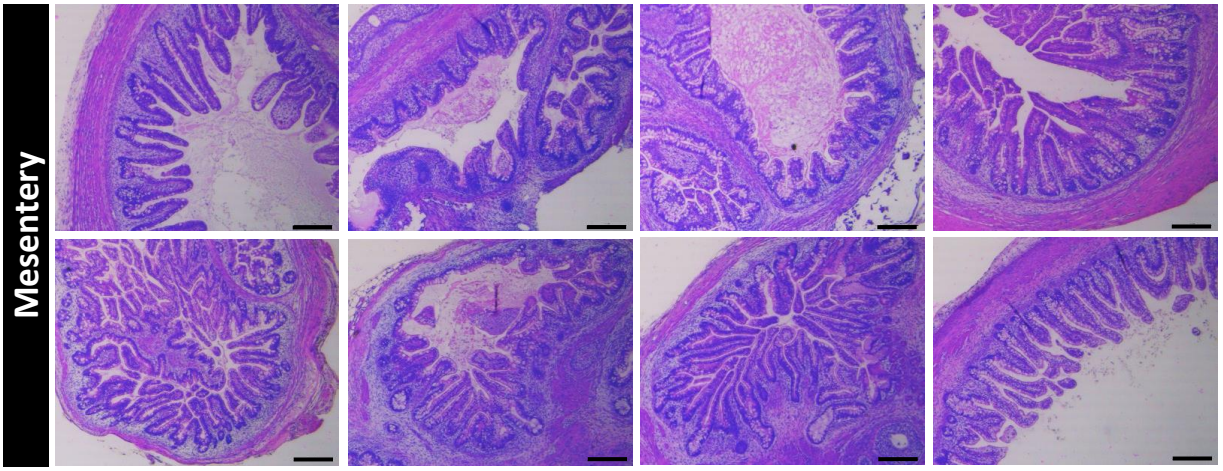

B.

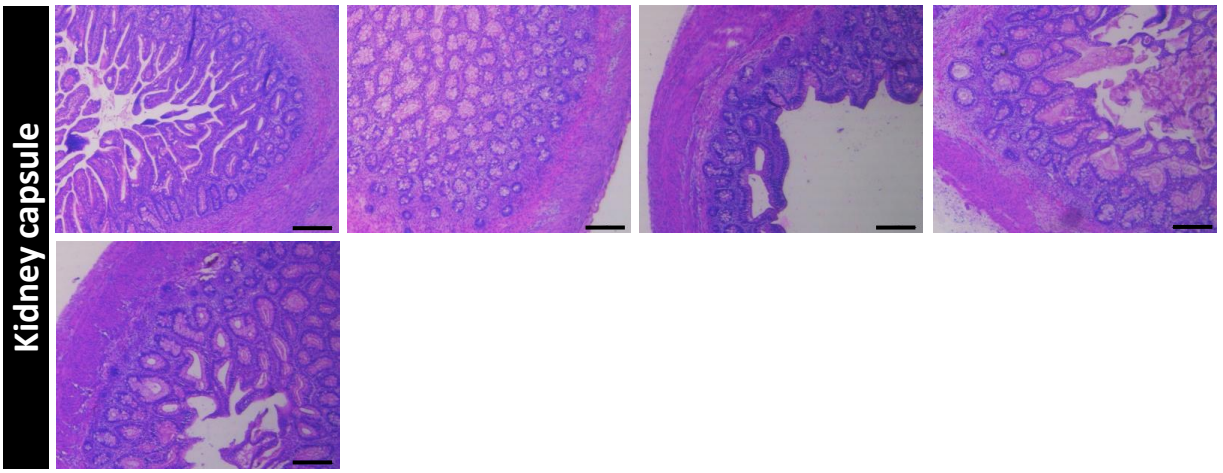

C.

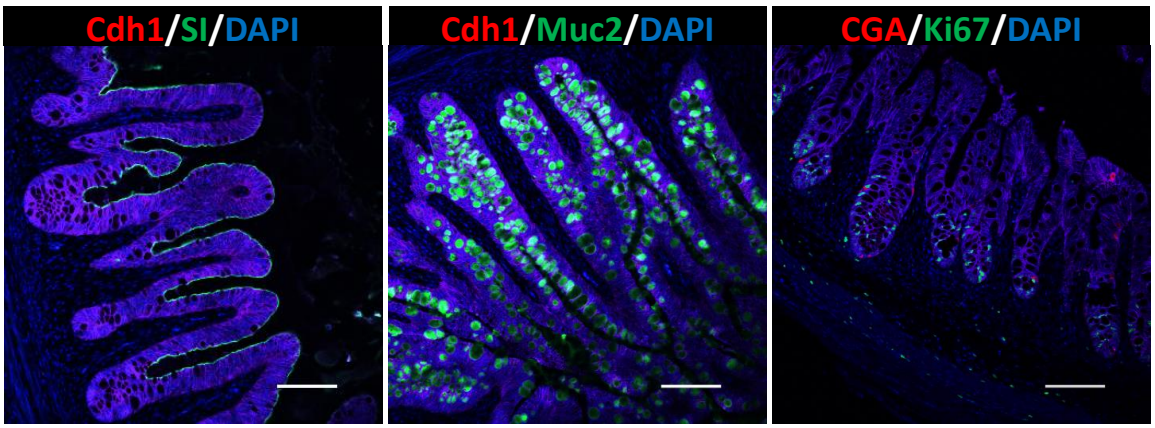

Figure S6, related to Figure 6

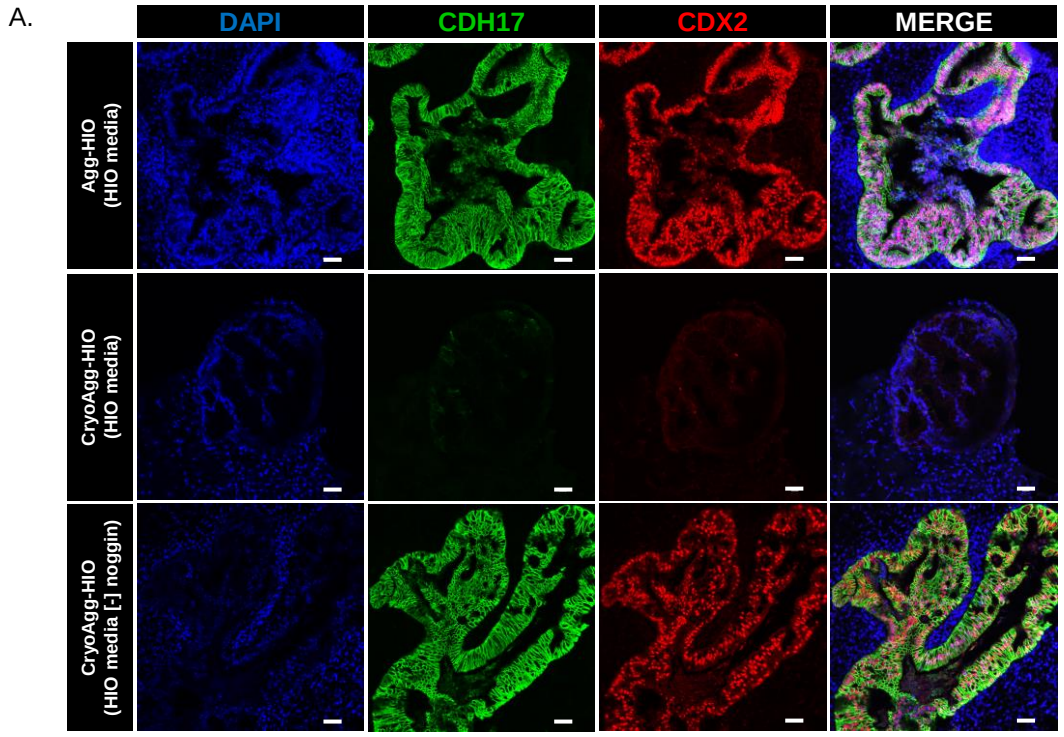

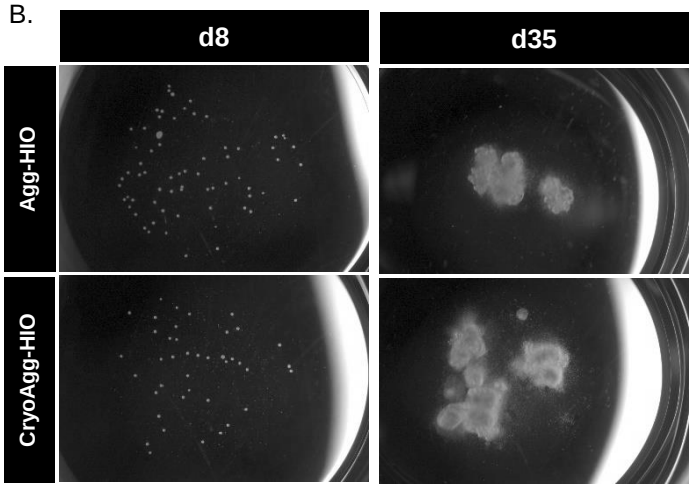

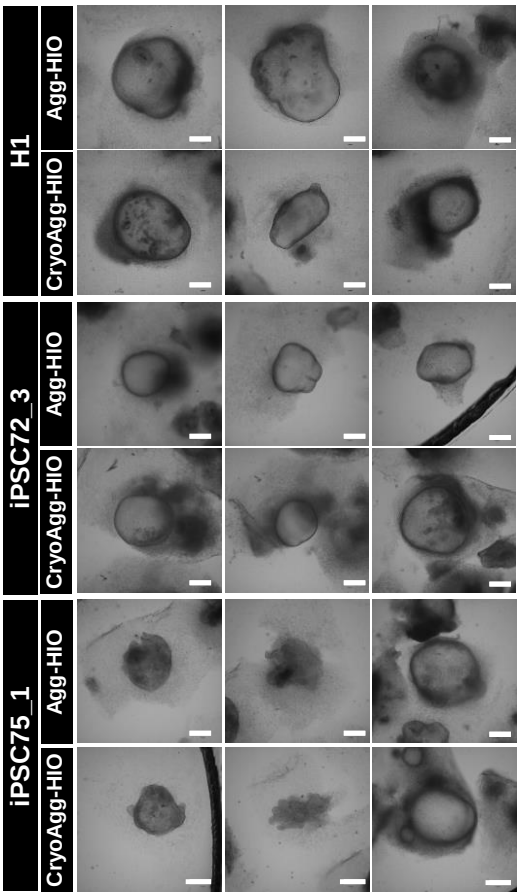

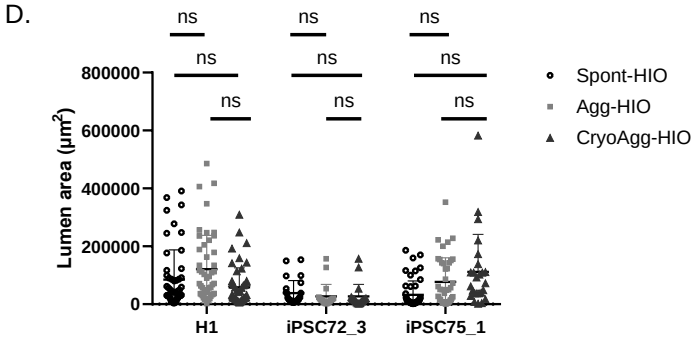

Figure S7. related to Figure 7

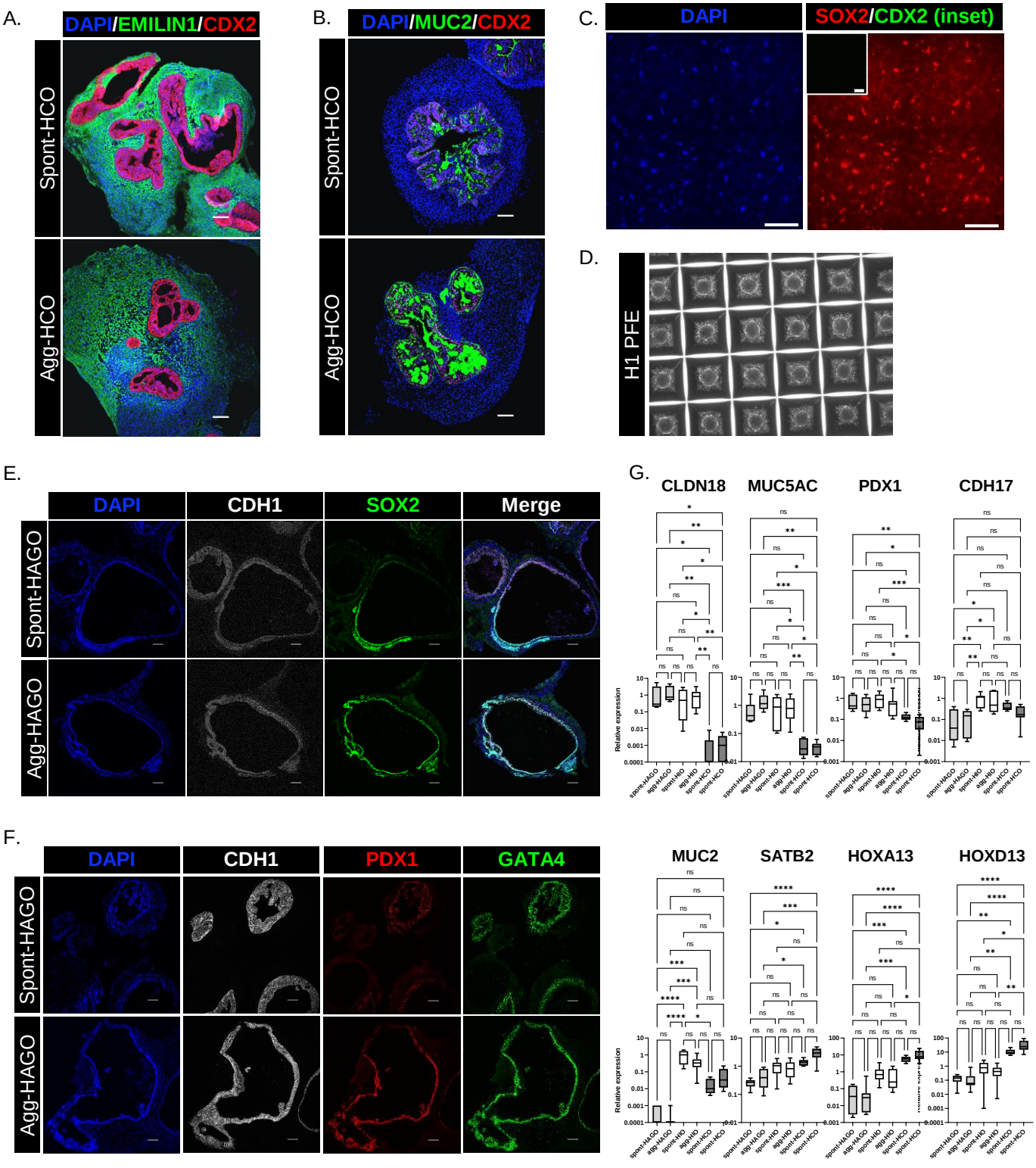

Supplemental Figure Legends

Supplemental Figure 1

Quality control analysis of hPSCs used in this study. Cryopreserved working banks of all hPSCs lines (H1, iPSC72_3, iPSC75_1, iPSC115_1, and iPSC285_1) were simultaneously generated and subjected to quality control assessment before use in the study. Following thaw, cells were maintained in culture for a maximum of 20 passages before being discarded and a new vial thawed.

(A) Karyotype analysis: standard metaphase spreads and G-banded karyotype were processed and interpreted by the CCHMC cytogenetics core.

(B) Stemness marker analysis: hPSC cultures were co-stained with FITC-conjugated anti-Tra-1-60 and Alexa Fluor-conjugated anti-SSEA4 antibodies and analyzed by flow cytometry. Negative (T-/S-), Tra1-60+ (T+/S-), SSEA4+ (T-/S+), and double positive (T+/S+) populations are shown.

(C) Cell line identity authentication assessment by STR: DNA from H1 hESCs, donor cells used to make iPSC lines used in the study, and iPSCs was subjected to STR analysis of 16 genetic loci. STR profile of donor cells matched STR profile of derived iPSCs.

(D) Analysis of functional pluripotency of hPSC lines used in the study. Total RNA was harvested from undifferentiated hPSCs and D14 embryoid bodies (EB) derived from each line and subject to Scorecard assay. The Scorecard assay identifies germ layer-specific differentiation potential *in vitro* by quantifying the expression of 94 defined self-renewal, ectodermal, mesodermal, endodermal genes by Taqman qRT-PCR in undifferentiated and embryoid body samples (Tsankov *et al.*, 2015). Expression data from each line is uploaded to a proprietary cloud-based data analysis tool which generates an algorithm score (top panel) and

an overall assessment of trilineage potential (bottom panel) for each line. Top panel: The algorithm score permits assessment of the change in expression of linage-specific genes during EB differentiation as well as comparison to the expression of those genes in 13 undifferentiated reference hPSC lines. Bottom panel: a [+] icon for a given germ layer indicates that the expression profile predicts differentiation potential for that germ layer, [o] indicates borderline ability to differentiate into that germ layer, and [-] indicates that a line may not be optimal for differentiating into that germ layer. Importantly, whilst endoderm scores for each line used in this study indicate different levels of endoderm potential, our data demonstrate that differences in Scorecard algorithm scores do not correlate to the ability of a given line to form uniformly CDX2+ MHE.

Supplemental Figure 2

(A) Undifferentiated H1, iPSC72-3, iPSC75_1, iPSC115_1 and iPSC285_1 cells were plated at equivalent seeding density for MHE generation and HIO production (McCracken *et al.*, 2011). Scale bar = 2 mm.

(B) A single cell suspension of undifferentiated H1 was plated at $1.5x10^5$ cells/well of a 24-well plate for MHE generation. The number of detached spont-spheroids per well for each experiment was quantified. N=3 experiments, *p=0.032, **p=0.002.

(C) D7 MHE derived from H1s plated as single cells was fixed and immunostained with antibodies to the MHE marker CDX2 (green) and counterstained with DAPI. = 100µm.

(D) Representative images of the gross morphology of H1-derived spont- and agg-HIOs at day 35. Scale bar = 500µm.

(E) iPSC115_1 cells were differentiated to d7 MHE and exhibited poor morphogenesis and no spontaneous spheroid detachment. MHE was aggregated and embedded in Matrigel on day 8

for HIO generation. Tiled image of a representative region on the d7 MHE morphology showing poor MHE morphogenesis and no detached spont-spheroids. Scale bar = 500µm.

(F) iPSC115_1 MHE monolayers were fixed and immunostained with antibodies to MHE marker CDX2 and foregut endoderm marker SOX2. Undifferentiated iPSC115_1 cells served as $CDX2^-$ /$SOX2^+$ controls. Cells were counterstained with DAPI. Scale bar = 100µm.

(G) Image showing aggregation of iPSC115_1 derived MHE ~16 hours after plating in an Aggrewell 400 plate.

(H) Day 35 iPSC115_1 agg-spheroid-derived HIOs were fixed, embedded in paraffin and sectioned. Sections were subjected to immunostaining with antibodies to CDX2 and CDH17 (intestinal epithelia) and Emilin1 (mesenchyme). Scale bars = 200µm.

Supplemental Figure 3

(A) Three iPSC lines were differentiated to MHE and after collection of spont-spheroids, the MHE monolayer was aggregated. Resulting day 8 aggregates were imaged 16 hours later. Left panel scale bar = 500µm. Right panel scale bar = 100µm.

(B) H1 cells were differentiated to MHE and detached spont-spheroids from all wells were collected. The remaining monolayer was then aggregated and collected. All collected spont- and agg-spheroids were plated in separate wells of a 2-well cell culture chamber slide and images were captured on a Keyence model BZ-X710. Images were tiled to show the complete imaged area of each chamber slide. Scale bar = 2.5 mm.

(C) Calculation of spont- and agg-spheroid area. Keyence BZ-X800 Analyzer software was used to count and define the perimeter of each spheroid not touching the edge of each frame from each frame captured in Fig. S4B. The perimeter was then used to calculate the area of each

spheroid. Left: representative example of a single captured image of spont- and agg-spheroids. Scale bar = 100µm. Right: the same frame showing the count (cyan) and area (gray) of each spheroid generated by the BZ-X800 Analyzer software.

(D) Comparison of spont- and agg-spheroid area consistency. Spheroid area (μm^2) was calculated as described in Fig. S4C and the percentage of total spont-spheroids (black) and agg-spheroids (gray) with an area within each range is shown.

Supplemental Figure 4

(A) Spont-spheroids and Agg-spheroids were generated from iPSC72_3, iPSC75_1 and iPSC285_1 and embedded in Matrigel. Representative images of gross morphology were captured after 3 days culture in Matrigel. Scale bar = 100µm.

(B) Spont- and agg-spheroids were generated from H1 hESCs. On day 28 representative images of gross organoid morphology were captured. Scale bar = 200µm.

(C) Total RNA was isolated from H1-derived d7 spont- and d8 agg-spheroids, and spont- and agg-HIOs. Taqman qRT-PCR was used to assess the expression of intestinal differentiation markers. Relative expression indicates fold-change vs. spont-spheroid. Data is expressed as mean ± SEM (n=3 experiments, 3 wells each *P<0.05 **p<0.01, ***p<0.001, NS = not significant).

(D) Sections from H1-derived spont- and agg-HIOs were stained with DPP4 antibodies and counterstained with DAPI. Representative epithelial DPP4 expression is shown. Scale bar = 100µm.

Supplemental Figure 5

Day 35 agg-HIOs were transplanted to the mesentery and kidney capsule of immunodeficient NSG mice.

(A) Agg-HIOs transplanted to the mesentery were harvested after 62 days for analysis. Organoids were fixed, embedded in paraffin, sectioned and subject to H&E staining. Representative sections of each engrafted organoid are shown. Scale bars = 200μm.

(B) Agg-HIOs transplanted to the kidney capsule were harvested after 83 days for analysis. Organoids were fixed, embedded in paraffin, sectioned and subject to H&E staining. Representative sections of each engrafted organoid are shown. Scale bars = 200μm.

(C) Sections from agg-HIOs transplanted to the mesentery were immunostained for intestinal epithelial markers SI (enterocyte), MUC2 (goblet cells), and CHGA (enteroendocrine cells). Proliferative cells were also detected by immunostaining for KI67. Scale bars = 100μm.

Supplemental Figure 6

HIOs were generated from MHE that was processed to single cells, cryopreserved, and then aggregated (CryoAgg-HIO).

(A) Control spont- and agg-spheroids were cultured in HIO media containing NOGGIN. Agg-spheroids generated from cryopreserved MHE were cultured in HIO media either containing [+] or lacking [-] NOGGIN. Sections of day 35 organoids were immunostained with antibodies to CDH17 and CDX2 and counterstained with DAPI. Representative images are shown. Scale bars = 50μm.

(B) Representative morphology of developing HIOs generated from control aggregated MHE (top) and following cryopreservation, thaw, and aggregation (bottom).

(C) Representative images of H1, iPSC72_3 and iPSC75_1-derived Agg- and cryoAgg-HIOs (d35). Scale bar = 500µm.

(D) Randomly selected Agg- or cryoAgg-HIO sections were imaged and the lumen area of each organoid measured using Nikon Elements software by manually defining the area of each lumen. Two Way ANOVA with Tukey's Post Hoc analysis was used to assess statistical significance. N=3 experiments, NS = not significant.

Supplemental Figure 7

Generation of colonic and antral gastric organoids by aggregation of patterned endoderm progenitors.

(A) Posteriorized MHE aggregates generate organoids (Agg-HCO) containing epithelial and mesenchymal layers. H1-derived MHE spont- and agg-spheroids were patterned to posterior hindgut MHE-derived spont- and agg-spheroids were exposed to BMP2 (Munera *et al.*, 2017) and cultured to day 35. Sections were co-immunostained with antibodies to CDH1 (epithelia) and Emilin1 (mesenchyme). Scale bar = 100µm.

(B) Agg-HCOs contain intestinal epithelia and goblet cells. Day 35 agg-HCOs were immunostained with antibodies to CDX2 (intestinal epithelia) and MUC2 (goblet cells). Scale bar = 100µm.

(C) Generation of $SOX^{+}/CDX2^{-}$ foregut endoderm. H1-derived DE was patterned to posterior foregut endoderm (PFE) (McCracken *et al.*, 2014) and co-immunostained for the foregut marker SOX2 and hindgut marker CDX2. Cells were counterstained with DAPI. Four tiled images from adjacent, randomly selected fields are shown. Scale bar = 1 mm.

(D) Aggregate formation from posterior foregut endoderm (PFE) monolayers. H1-derived PFE was harvested to single cells by exposure to accutase and aggregated in Aggrewell 400 plates.

A representative image of uniform PFE aggregates formed 16 hours after plating is shown. Scale bar = 500µm.

(E) PFE aggregates generate organoids (Agg-HAGO) containing foregut epithelia. Spontaneous PFE spheroids and PFE aggregates were embedded in Matrigel and cultured to day 33. Sections of organoids were immunostained to identify foregut epithelia ($CDH1^+/SOX2^+$). Scale bar = 100µm.

(F) Agg-HAGO epithelia has posterior foregut identity. Sections from day 35 spont- and agg-HAGO organoids were co-immunostained with antibodies to epithelia (CDH1) and the posterior foregut markers PDX1 and GATA4. Sections were counterstained with DAPI. Scale bar = 100µm.

(G) Expression of gut segment specific markers was assessed by qRT-PCR in D35 spont- and agg-HAGOs, -HIOs, and -HCOs. Expression of each gene was normalized to HIO-spont (n=3 experiments, 3 wells each; *p< 0.05, **p< 0.01, ***p<0.001, ****p<0.0001).

Supplemental Tables

Table S1: Antibodies used in this study.

Primary antibodies	**Vendor**	**Catalog #**	**Dilution**
Mouse anti-CDH1	BD Biosciences	610182	1:500
Mouse anti-CDH1	Abnova	PAB12286	1:500
Goat anti-CDH1	R&D Systems	AF648	1:500
Rabbit anti-CDH17	Sigma	HPA023616	1:500
Rabbit anti-CDX2	Cell Marque	235R-14	1:500
Mouse anti-CDX2	Biogenix	Mu392A-UC	1:500
Mouse anti-CHGA	Abnova	H00009545-A01	1:500
Mouse anti-CHGA	DHSB	CPTC-CHGA-3	1:500
Rabbit anti-CLDN18	Atlas	HPA018446	1:500
Goat anti-DPP4	R&D Systems	AF954	1:200
Rabbit anti-Emilin1	Atlas	A116271	1:400
Goat anti-FOXF1	R&D Systems	AF4798	1:500

Rabbit anti-GATA4	Santa Cruz	sc-9053	1:500
Rabbit anti-Ki67	Abnova	PAB20694	1:300
Rabbit anti-MUC2	Abcam	ab134119	1:1250
Mouse anti-MUC5AC	Abcam	Ab3649	1:250
Goat anti-PDX1	Abcam	47383	1:100
Rabbit anti-SATB2	Cell Marque	384-R15	1:100
Goat anti-SOX2	Santa Cruz	sc-17320	1:500
Mouse anti-SSEA4-alexafluor 647	Biolegend	330407	1:40
Rabbit anti-Sucrose Isomaltase	Atlas	HPA011897	1:1000
Mouse anti-Tra-1-60-FITC	BD Pharmingen	560876	1:20
Secondary antibodies	**Vendor**	**Catalog #**	**Dilution**
Alexafluor donkey anti-goat 488	ThermoFisher	A-11055	1:1000
Alexafluor donkey anti-goat 568	ThermoFisher	A-11057	1:1000
Alexafluor donkey anti-goat 647	ThermoFisher	A-21447	1:1000
Alexafluor donkey anti-mouse 488	ThermoFisher	A-21202	1:1000
Alexafluor donkey anti-mouse 568	ThermoFisher	A-10037	1:1000
Alexafluor donkey anti-mouse 647	ThermoFisher	A-31571	1:1000
Alexafluor donkey anti-rabbit 488	ThermoFisher	A-21206	1:1000
Alexafluor donkey anti-rabbit 568	ThermoFisher	A-10042	1:1000
Alexafluor donkey anti-rabbit 647	ThermoFisher	A-31573	1:1000

Table S2: Taqman probes used in this study.

Gene	Gene Name	Gene ID	TaqMAN #	Accession #
ACTB	Beta-actin	60	Hs01060665_g1	NM_001101.3
CHGA	Chromogranin A	1113	Hs00900375_m1	NM_001275.3
DPPIV	Dipeptidylpeptidase 4	1803	Hs00175210_m1	NM_001935.3
LGR5	Leucine Rich Repeat Containing G Protein-Coupled Receptor 5	8549	Hs00969422_m1	NM_001277226.1
LYZ	Lysozyme	4069	Hs00426232_m1	NM_000239.2
MUC2	Mucin 2	4583	Hs03005103_g1	NM_002457.2
OLFM4	Olfactomedin 4	10562	Hs00197437_m1	NM_006418.4
VIM	Vimentin	7431	Hs00185584	NM_003380.3

Supplemental References

McCracken et al., 2011. Generating human intestinal tissue from pluripotent stem cells in vitro.

Nat Protoc 6, 1920-1928. 10.1038/nprot.2011.410.

McCracken et al., 2014. Modelling human development and disease in pluripotent stem-cell-derived gastric organoids. Nature 516, 400-404. 10.1038/nature13863.

Munera et al., 2017. Differentiation of Human Pluripotent Stem Cells into Colonic Organoids via Transient Activation of BMP Signaling. Cell Stem Cell 21, 51-64 e56. 10.1016/j.stem.2017.05.020.

Tsankov et al., 2015. A qPCR ScoreCard quantifies the differentiation potential of human pluripotent stem cells. Nat Biotechnol 33, 1182-1192. 10.1038/nbt.3387.